EXPERIMENTAL STUDY OF AN ULTRA-HIGH-SPEED ORC TURBOGENERATOR

Tomasz Z. Kaczmarczyk[1]*, Grzegorz Żywica[1], Paweł Bagiński[1], Artur Andrearczyk[1]

[1]Institute of Fluid Flow Machinery, Polish Academy of Sciences, Department of Turbine Dynamics and Diagnostics, Gdańsk, Poland

*Corresponding Author: tkaczmarczyk@imp.gda.pl

ABSTRACT

This paper presents the results of an experimental study carried out on a 1-kilowatt microturbogenerator prototype with a maximum rotational speed of 120,000 rpm. The microturbogenerator prototype has a hermetic structure and was built using oil-free technology involving the use of gas bearings. The bearings are supplied with the vapour of the low-boiling liquid HFE7100. The work presents the results of the tests performed on the microturbogenerator at a heat source power of 14 kW_t and 20 kW_t. The tests were carried out at a fixed flow rate of the working fluid and a varying electric load of the generator. One of the main objectives of the study was to check in which ranges of the thermodynamic parameters the microturbogenerator can operate correctly. The electrical power measured at the outlet of the ORC system was found to increase with the power of the heat source and the flow rate of the working fluid. It was also found that the maximum electrical power produced by the ORC system strongly depends on the load of the microturbine generator. A maximum electrical output power of 639 W_e of the ORC system was obtained with a thermal power of the heat source of 20 kW_t and a flow rate of HFE7100 of 60 g/s. A maximum isentropic efficiency of about 72% was achieved by the microturbogenerator at a HFE7100 flow rate of 30 g/s and a heat source power of 14 kW_t.

1 INTRODUCTION

The continuous increase in demand for electricity (Pablo-Romero *et al*., 2017) and increasingly stringent environmental requirements have made it necessary to undertake actions aimed at increasing the efficiency of existing and newly built power systems (Lund *et al.*, 2020). At present, green energy technologies that use renewable fuels are being promoted. One technology that is in line with the current trends is CHP-ORC systems, which are constantly being developed by research teams around the world (Eyerer *et al.*, 2020). Despite the very intensive development of ORC technology which has been going on for over a decade now, there is still limited availability of microexpanders with power below 3 kW_e in the commercial market (Kaczmarczyk *et al.*, 2020a). In order to meet current market and environmental requirements, a microturbogenerator has been designed and built (Kaczmarczyk *et al.*, 2019) and is currently the subject of our research. In addition, volumetric machines such as compressors and pumps are often used as expanders for CHP-ORC systems (Wołowicz *et al.*, 2021). However, it should be noted that one of the disadvantages of most volumetric machines is the need for additional bearing lubrication systems, which can reduce the power output of the ORC system even by up to 5% (Weiß *et al.*, 2018). Currently, research is underway on the use of ORC systems in energy-efficient buildings (Mascuch *et al.*, 2021) and mobile applications (Pili *et al.*, 2017). The main problem with using ORC systems in mobile applications is their weight, which should be as low as possible, resulting in energetic and economic benefits (Wu *et al.*, 2020). Most volumetric expanders have a low specific speed and are usually equipped with slow-speed generators (Jang and Lee, 2019), which consequently make them several times heavier than high-speed microturbines (Uusitalo *et al.*, 2020). In addition, flow expanders offer much lower noise and vibration levels than volumetric expanders, which is important when it comes to using ORC systems in the building industry (Kaczmarczyk et al. 2016). Thus, in order to extend the application possibilities of expansion machines, they must be as light as

possible and have a wide operating range and high efficiency. However, it is important to note that when high-speed generators are used in expansion machines, it is necessary to design a special bearing system for the shaft and manufacture the rotating elements of the microturbine with appropriate precision (Żywica *et al.*, 2020).

To meet the above-mentioned requirements, an ultra-high-speed turbogenerator with a power capacity of 1 kW_e and a maximum rotational speed of 120,000 rpm was designed and built. Thanks to the use of gas bearings that are lubricated by the working fluid, the microturbine has a hermetically sealed structure, so it does not require any lubricants and its vibration level is low. Preliminary studies described in the article by (Kaczmarczyk *et al.*, 2020b) show that the microturbogenerator can produce a power of about 1.1 kW_e at nominal operating parameters. A universal expander must be able to function properly over a wide range of thermodynamic parameters. This paper therefore presents the results of the experimental research carried out on the microturbogenerator whose operating parameters were lower than their nominal values. The objective of the research was to verify the technical condition of the microturbogenerator over a wide operational range. The tests were carried out at different capacities of the heat source and at fixed flow rates of the working fluid. The way in which the generator load affects the electrical power produced by the microturbogenerator was studied. Interestingly, the very low electrical power and very high rotational speed of the tested microturbogenerator are very similar to those obtained for gas microturbines and small jet engines. The research results presented in this paper constitute a novelty in the field of CHP-ORC systems and may fill the existing gap in the literature.

2 TEST RIG

The tests of the microturbogenerator prototype were carried out on a test rig whose diagram is shown in Fig. 1. The instantaneous electric induction heater with a maximum power of 48 kW_e was used as the heat source.

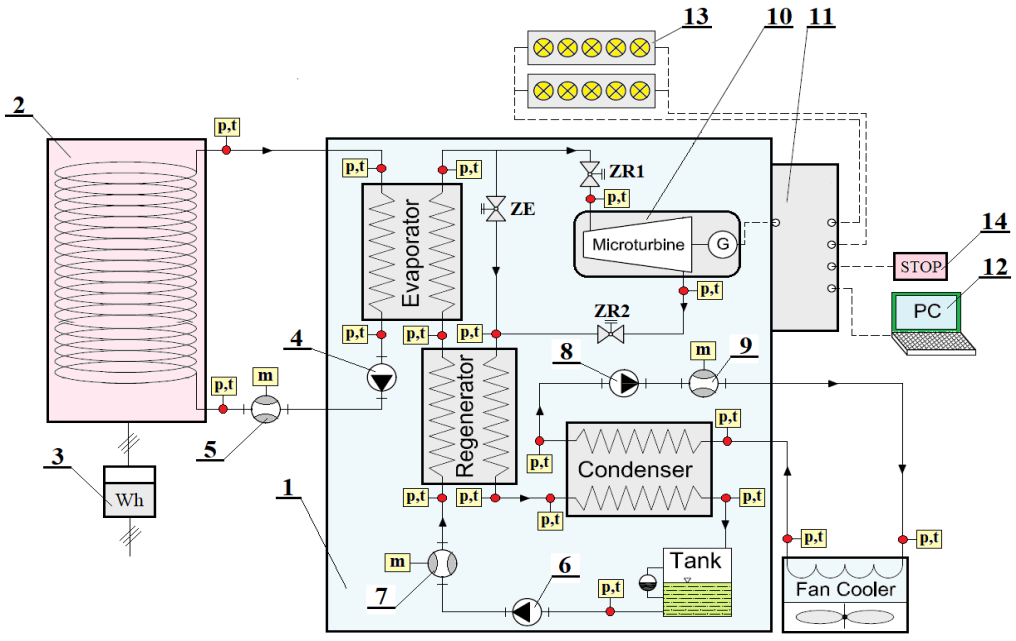

Figure 1: Test rig diagram: 1 – installation with heat exchangers, 2 – electric thermal oil heater, 3 – electricity meter, 4 – oil pump, 5 – ultrasonic flowmeter, 6 – working fluid pump, 7 – Coriolis mass flowmeter, 8 – cooling system pump, 9 – turbine flowmeter, 10 – microturbogenerator, 11 – electric energy conditioning system, 12 – measuring computer, 13 – electrical load system, 14 – emergency switch, (p, t – pressure measuring point and temperature pressure measuring point, m – flow rate measuring point, ZE – expansion valve, ZR – control valve)

The electric heater is equipped with a PID controller that regulates the oil temperature with an accuracy of ±1°C. The power of the heater can be smoothly regulated with an accuracy of 0.1 kW over the entire operating range using a potentiometer. The circulating thermal oil is heated by the electric heater and then directed to the evaporator. During the ORC installation heating process, the HFE7100 working fluid is directed to the regenerator using the expansion valve (ZE), then to the condenser. After its condensation, the working fluid is directed to a tank from where it is directed to the regenerator by means of a pump, and then to the evaporator. After the fluid has evaporated in the evaporator and its appropriate operating parameters (pressure and temperature) have been obtained, it is directed to the microturbogenerator. Valves ZR1 and ZR2 are then open and valve ZE is closed. The heat from the condenser is dissipated by a 50 kW_t fan cooler, which is equipped with a water spray system. The electric generator was loaded with a specially designed AC/DC rectifier prototype equipped with a resistive load system, composed of ten DC bulbs with a total capacity of 2,000 W. A diagram showing how the electrical load system is connected to the microturbine generator is presented in Fig. 2.

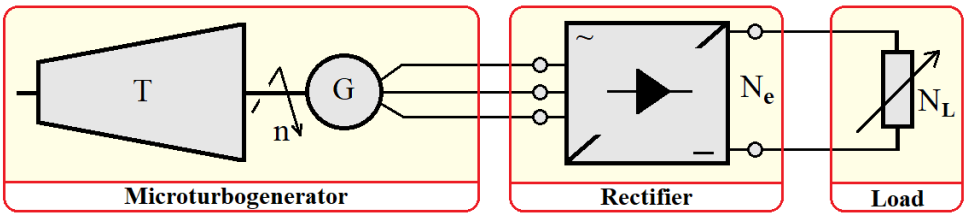

Figure 2: Diagram of the electrical load system of microturbine generator; T – microturbine, G – three-phase synchronous generator with permanent magnets, N_e – electrical power at the output of the rectifier, N_L – rated power of electrical load system

The generator load can be regulated by individually turning the bulbs on/off via switches. The electric current and voltage of the generator of the microturbine were measured at the outlet of the AC/DC rectifier. It is important to note that the test rig is quite universal as it allows testing of expansion machines with a power capacity between 3 and 5 kW_e. Therefore, a complete description of the test rig, as well as a description of the control and measurement apparatus, can be found in the paper (Kaczmarczyk *et al.*, 2019).

2.1 Microturbogenerator

The prototype of a single-stage axial-flow 1-kilowatt microturbine with partial admission was the object of the study. The image and 3D model of this microturbine are shown in Fig. 3.

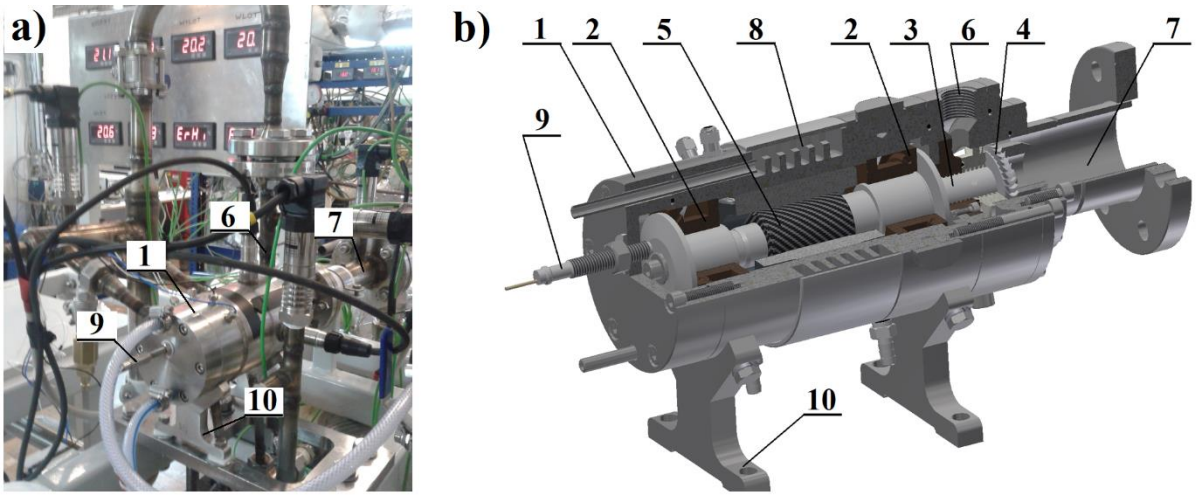

Figure 3: Photo (a) and 3D model (b) of the microturbogenerator: 1 – housing, 2 – gas bearing, 3 – shaft, 4 – vane disc, 5 – generator rotor with permanent magnets, 6 – feed channel, 7 – discharge channel, 8 – generator cooling system, 9 – rotational speed sensor, 10 – support

The microturbogenerator shaft, supported by two gas bearings, is located inside the housing, which has an outer diameter of 90 mm and a length of 190 mm. The selected geometrical parameters of the microturbine flow system are shown in Table 1.

Table 1: Geometrical parameters of the single-stage axial-flow microturbine

Parameter	Stator	Rotor
Number of blades	3	35
Blade height	2.9	3.3
Minimum distance between blades	0.5	0.9
Partial admission ratio	29%	-
Outer diameter of rotor	-	36.2

A vane disc and a generator rotor with permanent magnets are mounted on the shaft. The machine is equipped with a three-phase synchronous generator with a maximum speed and power of 120,000 rpm and 1.5 kW_e respectively (Kaczmarczyk *et al.,* 2020b). The design operating pressure of the working fluid (HFE7100) at the inlet and outlet of the microturbine was 1,035 kPa(a) and 102 kPa(a) respectively. At the microturbine inlet, the temperature was approximately 165°C and the flow rate was 0.071 kg/s. The Mach number at the outlet of the nozzle and rotor was 1.85 and 1.17 respectively. At a nominal rotational speed of 100,000 rpm and an electrical power of 1.17 kW_e, the microturbine had an internal efficiency of about 75%.

2.2 Measurement procedure

First, power was set on the electric thermal oil heater and the required flow rates of the working fluids, i.e. thermal oil, working fluid and coolant (ethylene glycol), were set using inverters. Both the electric power of the heater ($N_{e\text{-}HS}$) and the electric power of the cooling system was constant during the measurement of all operating characteristics. That is, during each series of measurements, $N_{e\text{-}HS}$, $N_{t\text{-}CS}$ and the flow rate of the working fluid were constant and only the load of the generator of the microturbine had been modified. Each series of measurements started with the lowest flow rate which was constant during the time when the electrical load characteristics (N_L) of the microturbine generator were obtained. A set of 10 bulbs connected in parallel was used as an electrical load for the generator of the microturbine. The load of the generator was first set to a maximum value and once the rotational speed of the microturbogenerator had been held for about 3 minutes, it was gradually reduced to the minimum value (i.e. a single 200-watt bulb). The electrical load of the generator was manually controlled using separate switches for each bulb. A maximum electrical load of 2,000 W_e of the microturbine generator was obtained with 10 connected bulbs. The electrical load was manually reduced by successively disconnecting 200-watt bulbs according to Table 2. The minimum electrical load of the generator protected the microturbine from an excessive increase in the rotational speed. The equivalent resistance (R_{eq}) of the electrical load system (with variable power of the receivers) was measured at an ambient temperature of 18.5°C using a digital oscilloscope made by Siglent (the model SHS810), which has an accuracy of ±1% MV.

Table 2: Characteristics of the electrical load system of the microturbine generator

No.	**10**	**9**	**8**	**7**	**6**	**5**	**4**	**3**	**2**	**1**
N_L [W]	2,000	1,800	1,600	1,400	1,200	1,000	800	600	400	200
R_{eq} [Ω]	2.1	2.3	2.5	2.9	3.4	4.0	4.9	6.4	9.3	18.2

where: No. – number of bulbs, N_L – rated power of the load system, R_{eq} – equivalent resistance.

Some microturbine load characteristics were obtained for different flow rates of the working fluid at constant values of the heat source power and cooling system power.

3 RESULTS OF EXPERIMENTAL RESEARCH

The microturbogenerator tests were carried out at a heat source power of 14 kW_t and 20 kW_t. For a thermal power of 14 kW_t, tests were performed for the following four average values of HFE7100 fluid flow rate: 30 g/s, 40 g/s, 50 g/s and 60 g/s. On the other hand, at a heat source power of 20 kW_t, measurements were performed for three flow rates of the HFE7100 fluid: 40 g/s, 50 g/s and 60 g/s. Figure 4 shows the rotational speed of the microturbogenerator versus time for several fixed values of HFE7100 fluid flow rate when the load of the generator had been decreased.

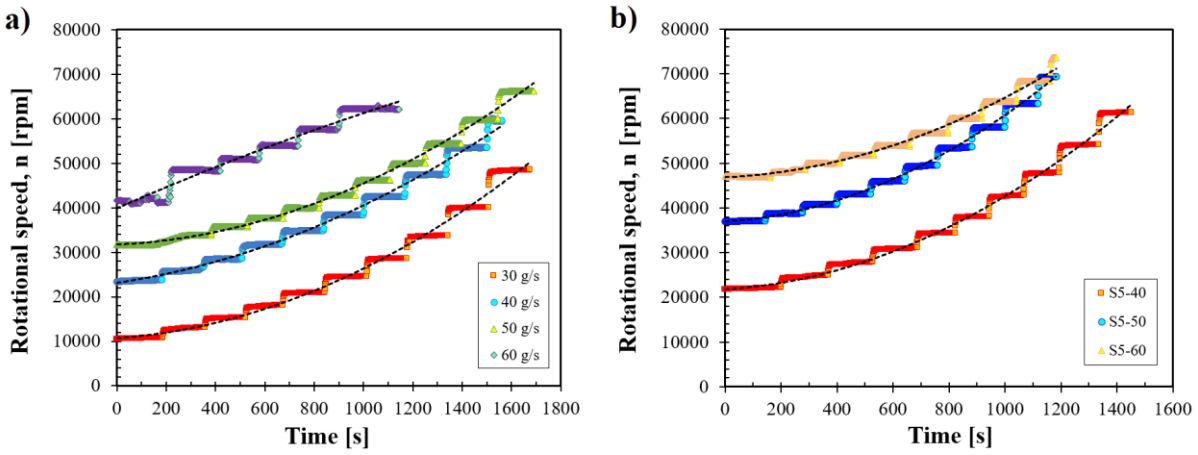

Figure 4: Graphs showing the rotational speed of the microturbogenerator measured for a heat source with a power of 14 kW_t (a) and 20 kW_t (b) versus time

Figure 4 shows that, independently of the power of the heat source, the rotational speed of the microturbogenerator increases when the flow rate of the working fluid increases. For example, at the maximum power of the receiver set (i.e. at a power of 2,000 W – Table 2), at a heat source power of 14 kW_t and at working fluid flow rates of 30 g/s, 40 g/s, 50 g/s and 60 g/s, the average values of the rotational speed of the microturbogenerator were respectively 10,690 rpm, 23,706 rpm, 31,567 rpm and 41,030 rpm. It is important to note that at a given generator load, the rotational speed of the microturbine was constant (Fig. 4).

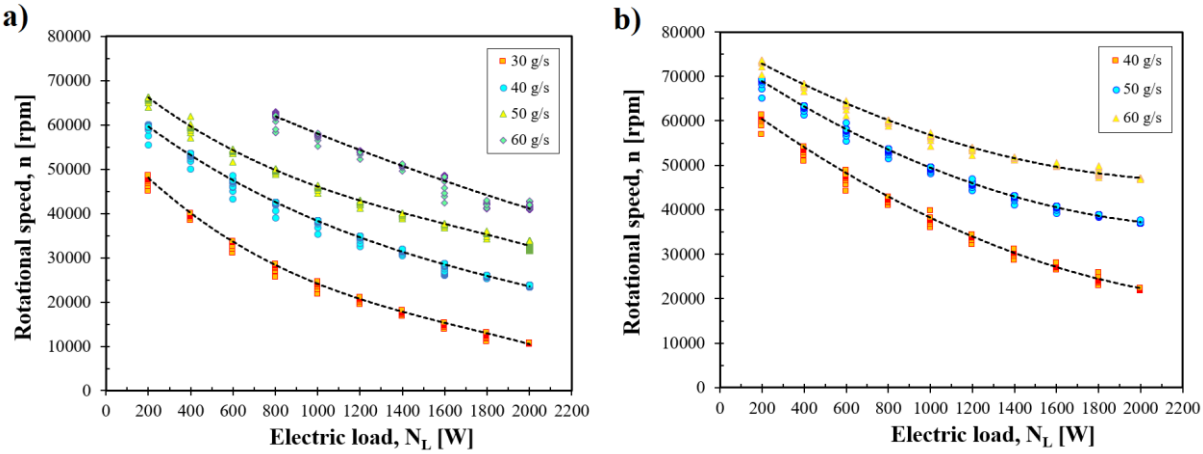

Figure 5: Rotational speed of the microturbogenerator versus rated power of electrical load system measured for a heat source with a power of 14 kW_t (a) and 20 kW_t (b)

Figure 5 shows that, regardless of the flow rate and power of the heat source, the rotational speed of the microturbogenerator increases when the electrical load of the generator decreases (Fig. 4). The decrease

in speed was caused by the increased braking torque that loaded the microturbine generator. It was observed that the fluid pressure and temperature gradients of the HFE7100 fluid measured before and after the microturbogenerator depended on the thermal power of the heat source, the flow rate and the nominal power of the generator. After analysing the thermodynamic parameters (pressure and temperature) measured at the inlet and outlet of the microturbogenerator (Table 3). It was found that the cooling rate of the working fluid at the machine inlet at a flow rate of 60 g/s (N_s=14 kW_t) was 33.84 °C/hour. The cooling of the fluid at the inlet (for N_s=14 kW_t at a flow rate of 60 g/s) causes the pressure to drop at a rate of 86.76 kPa(a)/h. This means that at a fluid flow rate of 60 g/s, the power of the heat source of 14 kW_t was too low to ensure adequate thermodynamic parameters at the inlet of the machine. This is shown by the power curve corresponding to a flow rate of 60 g/s (Fig. 5a), where the electrical output power of the ORC system decreased after the electrical load exceeded 1,400 W.

Table 3: Values of the temperature and pressure of the working fluid measured at the inlet and outlet of the microturbogenerator

		For N_s=14 kW_t				For N_s=20 kW_t		
		HFE7100 mass flow rate				HFE7100 mass flow rate		
Parameter	**Unit**	**30 g/s**	**40 g/s**	**50 g/s**	**60 g/s**	**40 g/s**	**50 g/s**	**60 g/s**
P_{in}	kPa(a)/h	*60.36*	*60.48*	*53.28*	*-86.76*	*118.44*	*52.56*	*10.80*
t_{in}	°C/h	*41.04*	*3.96*	*-16.92*	*-33.84*	*72.36*	*20.16*	*-11.88*
P_{out}	kPa(a)/h	*-0.36*	*-3.60*	*-5.40*	*-0.36*	*0.72*	*1.44*	*4.32*
t_{out}	°C/h	*32.76*	*-2.88*	*-21.60*	*-37.44*	*61.56*	*15.48*	*-13.68*

The supercooling of the working fluid, which takes place at the inlet of the microturbogenerator, results in a reduction of the output electrical power of the system (Fig. 6).

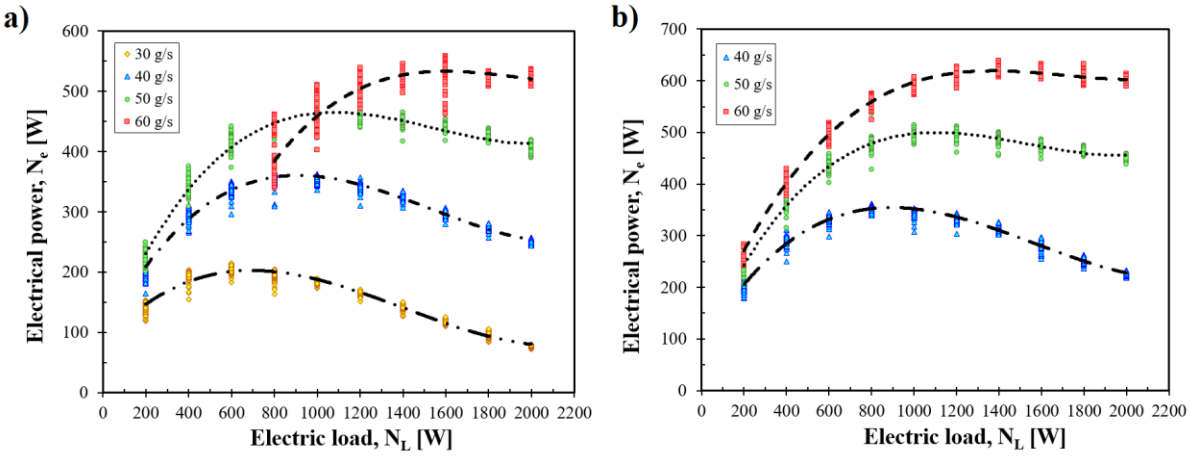

Figure 6: Electrical power of the microturbogenerator measured for a heat source with a power of 14 kWt (a) and 20 kWt (b) versus electrical load

Figure 6 shows that the output electrical power of the system increases with the flow rate of the working fluid, regardless of the power of the heat source. For example, at a heat source power of 14 kW_t and a maximum load of the generator, the average electrical power values at the system output at average flow rates of 30 g/s, 40 g/s, 50 g/s and 60 g/s were 90 W_e, 251 W_e, 413 W_e and 517 W_e, respectively. On the other hand, at a heat source power of about 20 kW_t and flow rates of 40 g/s, 50 g/s and 60 g/s, the output electrical power of the system was 227 W_e, 447 W_e and 599 W_e, respectively. It is worth noting that at a flow rate of 40 g/s, the output electrical power of the system was higher in the case where the power of the heat source was 14 kW_t. Table 2 shows that at a fluid flow rate of 40 g/s and a heat source power of 14 kW_t, the temperature measured at the inlet of the microturbogenerator increased

at a rate of 3.96 °C/h and at a heat source power of 20 kW_t, the temperature increased at a rate of 72.36 °C/h. It is important to mention that the microturbine has a hermetically sealed structure, which means that both the flow system of the microturbine and the generator are located inside the housing. When the blade system is supplied with the working fluid, the temperature rises in the area where the generator is mounted (i.e. the stator and the rotor with permanent magnets), and its maximum permissible operating temperature is 155 °C. However, the maximum temperature of the fluid, measured at the inlet of the microturbogenerator, was approximately 220 °C. To protect the generator from excessive temperature rise, the stator was cooled using tap water. It should be noted that too much cooling of the stator can cause condensation of the fluid in the gas bearings of the microturbogenerator, which in turn leads to their malfunction or even damage to the machine. Hence, the primary objective of the generator cooling system was to help achieve the lowest possible stator temperature while ensuring adequate superheating of the fluid that is supplied to the bearings and blade system. However, an increase in the temperature of the generator changes the resistance of the stator winding and causes a shift of the working point of the permanent magnet rotor on the demagnetisation characteristics, resulting in a decrease in electric power.

The temperature of the working fluid at the inlet of the microturbogenerator has an impact on both the electric current and the electric voltage of the synchronous generator of the microturbine (Fig. 7).

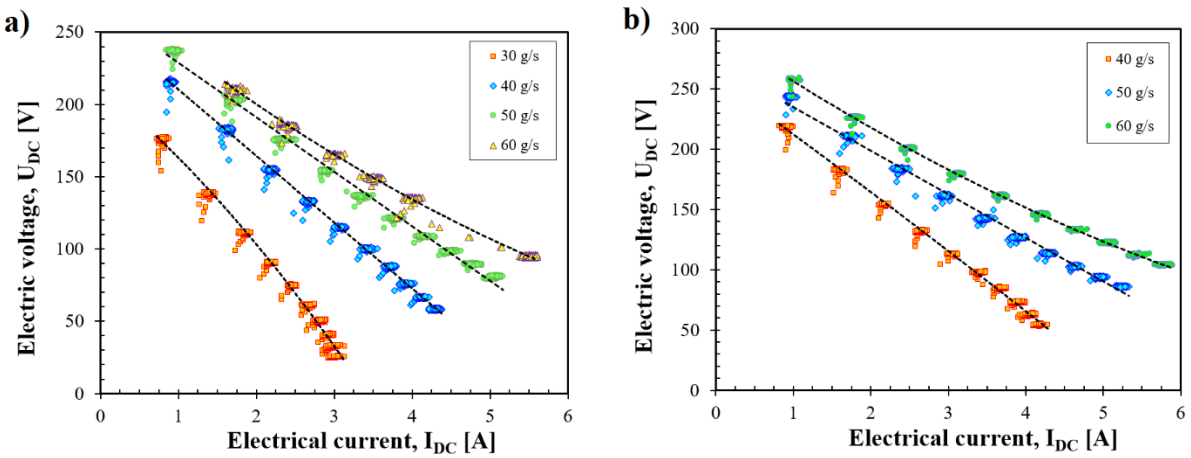

Figure 7: Electrical voltage and current of microturbogenerator measured for a heat source with a power of 14 kW_t (a) and 20 kW_t (b)

Figure 7 shows that, regardless of the power of the heat source, an increase in the temperature of the fluid at the inlet of the microturbogenerator leads to undercompensation of the synchronous machine (concave curve). The microturbine was uncompensated at flow rates of 30 g/s and 40 g/s (Figs. 7a and 7b). On the other hand, a decrease in the inlet temperature leads to overcompensation of the synchronous machine (convex curve). Overcompensation occurred at a flow rate of 60 g/s regardless of the power of the heat source. Overcompensation leads to the magnetization of the electric machine causing its self-excitation, which ultimately leads to its damage (Sołbut, 2019). In order for the output power of the cogeneration system to be as high as possible at fixed heat source parameters and fixed electrical load, the external characteristics of the synchronous generator must be perfectly compensated (straight line). The curves obtained at a working fluid flow rate of 50 g/s were almost ideally compensated (Figs. 5a and 5b). The load of the generator has a major influence on the output power of the system (Fig. 6). For a given power of the heat source and a given flow rate of the fluid, there is an optimal load of the generator at which the electrical output is maximum. For example, for a power of 20 kW_t and a working fluid flow rate of 40 g/s, the optimal value of the generator load was 800 W and it is at this value that the maximum electrical output of the system was registered (about 358 We). On the other hand, at the same power of the heat source and at a flow rate of 60 g/s, the maximum electrical output of the system (639 We) was registered at a generator load of 1,400 W. This suggests that the ORC system should be equipped with a control system which, based on the power of the heat source and the flow rate value,

should select the optimal value for the electrical load of the generator of the microturbine. The generator load should be selected so that the synchronous machine is as well compensated as possible.

The curves showing the isentropic efficiency versus the rotational speed and the electrical load of the microturbine generator are presented in Figs. 8 and 9, respectively. The isentropic efficiency was calculated from Eq. (1):

$$\eta_{is} = (h_1 - h_2)/(h_1 - h_{2s}) \tag{1}$$

where h_1 and h_2 stand for the enthalpy of the working fluid respectively before and after the microturbogenerator, and h_{2s} stands for the isentropic enthalpy of the HFE7100 vapour at the microturbine outlet.

Figure 8 shows that, regardless of the power of the heat source, the isentropic efficiency of the microturbogenerator decreases with the increase in the flow rate of the working medium. A maximum isentropic efficiency of 71.8% was obtained at a flow rate of 30 g/s and at a microturbine rotational speed of 39,778 rpm (Fig. 8a).

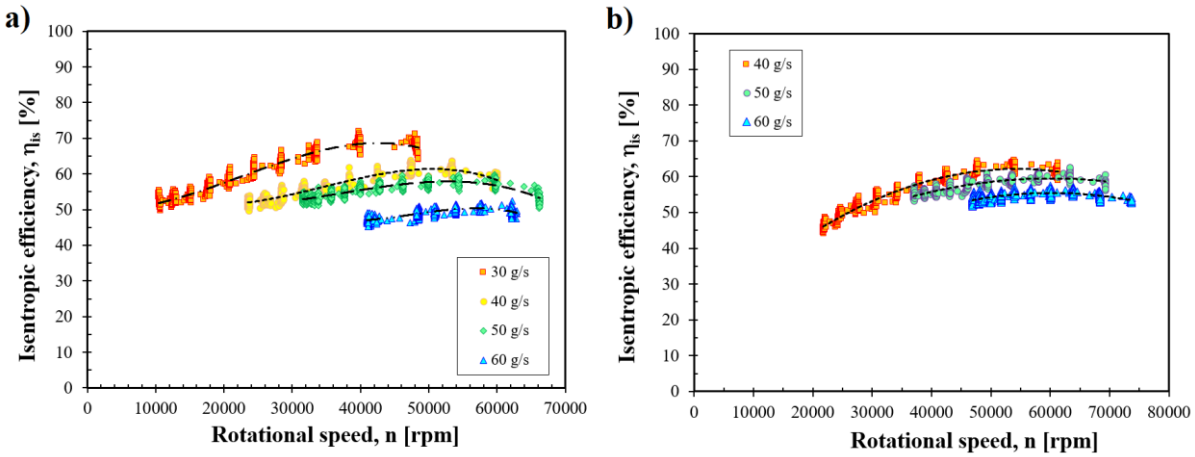

Figure 8: Isentropic efficiency versus the rotational speed of microturbogenerator for a heat source with a power of 14 kW_t (a) and 20 kW_t (b)

Regardless of the power of the heat source, the efficiency of the microturbine increased as the rotational speed of the microturbine increased until it reached a maximum value, and then decreased.

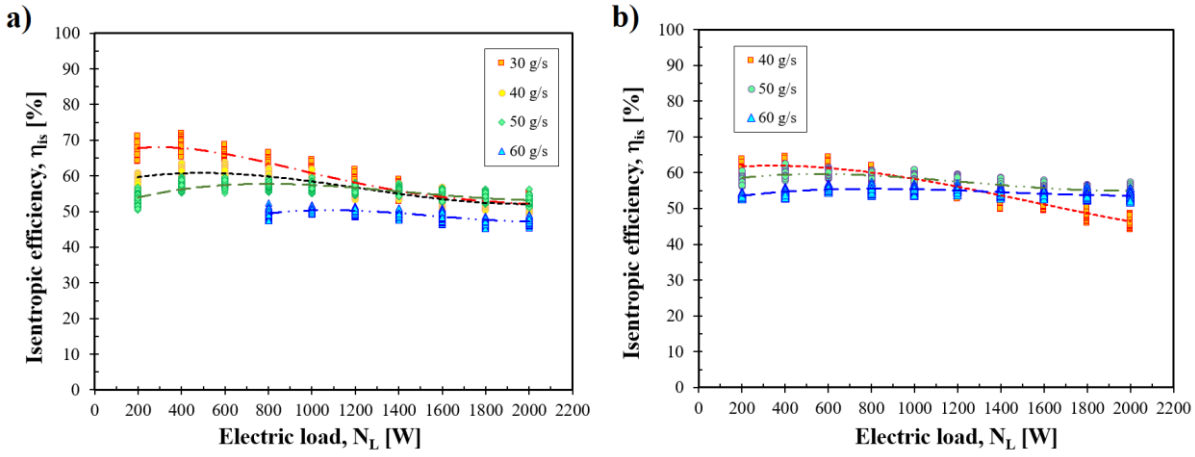

Figure 9: Isentropic efficiency versus the electrical load of microturbine generator for a heat source with a power of 14 kW_t (a) and 20 kW_t (b)

Figure 9 shows the isentropic efficiency versus the electrical load of the microturbine generator. Regardless of the flow rate of the working fluid, the isentropic efficiency of the microturbogenerator decreased with the increase in the electrical load of the generator. For a power of 20 kWt of the heat source and a flow rate of 60 g/s, the average isentropic efficiency of the microturbogenerator was practically constant and equal to 55%.

4 CONCLUSIONS

This paper presents an experimental study performed on a 1-kilowatt microturbogenerator, in order to verify the operating range where the thermodynamic parameters of the working fluid are different from the nominal operating conditions. It has been determined that in order to obtain the maximum electrical output of the cogeneration system at the fixed power of the heat source, both the flow rate of the working fluid and the power of the receivers used as load for the generator must be optimal. It has been found that the temperature of the fluid at the inlet of the microturbogenerator has a major influence on the electrical power produced and the proper operation of the synchronous generator. An increase in working fluid inlet temperature should be as low as possible so that the microturbine generator can be compensated. In order to determine the full operating characteristics of the microturbogenerator and the control curve of the system output power, it is necessary to carry out systematic tests over a wider range of heat source power. Based on these tests, it will be possible to determine the optimum values for the flow rates of the working fluid and the load of the generator.

NOMENCLATURE

I	current (A)
h	specific enthalpy (J/kg)
m	mass flow rate (g/s)
MV	measured value,
n	rotational speed (rpm)
N	power (W)
p	pressure (kPa)
R	resistance (Ω)
t	temperature (°C)
U	voltage (V)

Greek symbols

η	efficiency

Subscripts

1 – 2	state points
AC	alternating current
CS	cooling system
DC	direct current
e	electrical
eq	equivalent
HS	heat source
is	isentropic
L	load
t	thermal
wf	working fluid

REFERENCES

Eyerer S., Schifflechner C., Hofbauer S., Bauer W., Wieland C., Spliethoff H., 2020. Combined heat and power from hydrothermal geothermal resources in Germany: An assessment of the potential, *Renewable and Sustainable Energy Reviews*, vol. 120, no.109661.

Jang Y., Lee J., 2019, Comprehensive assessment of the impact of operating parameters on sub 1-kW compact ORC performance, *Energy Conversion and Management*, vol. 182, p. 369-382.

Kaczmarczyk T.Z., Żywica G., Ihnatowicz E., 2016, Vibroacoustic diagnostics of a radial microturbine and a scroll expander operating in the organic Rankine cycle installation, *Journal of Vibroengineering* 2016:18;4130-4147.

Kaczmarczyk T.Z., Żywica G., Ihnatowicz E., 2019, Experimental study of a low-temperature micro-scale organic Rankine cycle system with the multi-stage radial-flow turbine for domestic applications, *Energy Conversion and Management*, vol. 99, no. 111941.

Kaczmarczyk T.Z., Żywica G., Ihnatowicz E., 2020a, Experimental research on scroll expanders operating in parallel in an organic Rankine cycle system with a biomass boiler, *Energy Conversion and Management*, vol. 224, no. 113390.

Kaczmarczyk T.Z., Żywica, G., Baginski, P., Andrearczyk, A., 2020b, Preliminary experimental research of a 1 kW microturbine for micro-CHP applications. ECOS 2020 - Proceedings of the 33rd International Conference on Efficiency, Cost, Optimization, Simulation and Environmental Impact of Energy Systems. Osaka; Japan, 29 June - 3 July 2020: p. 847-858.

Lund H., Duic N., Østergaard P.A., Mathiesen B.A., 2020, Perspectives on Smart Energy Systems from the SES4DH 2018 conference, *Energy*, vol. 190, no.116318.

Mascuch J., Novotny V., Spale J., Vodicka V., Zeleny Z., 2021, Experience from set-up and pilot operation of an in-house developed biomass-fired ORC microcogeneration unit, *Renewable Energy*, vol. 165: p. 251-260.

Pablo-Romero M., del P, Pozo-Barajas R., Yñiguez R., 2017, Global changes in residential energy consumption, *Energy Policy*., vol. 101: p. 342-352.

Pili R., Romagnoli A., Kamossa K., Schuster A., Spliethoff H., Wieland Ch., 2017, Organic Rankine Cycles (ORC) for mobile applications – Economic feasibility in different transportation sectors, *Applied Energy*, vol. 204: p. 1188–1197.

Sołbut A., 2019, Maszyny elektryczne 2. Maszyny prądu stałego. Maszyny synchroniczne. Wydawnictwo Politechniki Białostockiej. Białystok 2019, p.120. (in Polish).

Uusitalo A., Turunen-Saaresti T., Honkatukia J., Dhanasegaran R., 2020, Experimental study of small scale and high expansion ratio ORC for recovering high temperature waste heat, *Energy*, vol. 208, no. 118321.

Weiß A.P., Popp T., Müller J., Hauer J., Brüggemann D., Preißinger M., 2018, Experimental characterization and comparison of an axial and a cantilever micro-turbine for small-scale Organic Rankine Cycle, *Applied Thermal Engineering*, vol. 40: p. 235-244.

Wołowicz M., Kolasiński P., Badyda K., 2021, Modern small and microcogeneration systems—a review, *Energies*, vol. 4, no. 3: p.785.

Wu X., Chen J., Lei Xie L., 2020, Optimal design of organic Rankine cycles for exhaust heat recovery from light-duty vehicles in view of various exhaust gas conditions and negative aspects of mobile vehicles, *Applied Thermal Engineering*, vol. 179, no. 115645.

Żywica G., Kaczmarczyk T.Z., Breńkacz Ł., Bogulicz, M., Andrearczyk, A., Bagiński, P., 2020, Investigation of dynamic properties of the microturbine with a maximum rotational speed of 120 krpm-predictions and experimental test, *Journal of Vibroengineering*, vol. 22, no. 2: p. 298-312.

ACKNOWLEDGEMENT

This paper was supported by the TechRol project that has received funding from the National Centre for Research and Development (NCBR); BIOSTRATEG strategic research and development programme under Grant Agreement No. BIOSTRATEG3/344128/12/NCBR/2017.